

INVESTIGATION OF VOLUME RECOMBINATION IN A HELIUM PLASMA IN A MAGNETIC FIELD

Yu. M. ALESKOVSKIĬ and V. L. GRANOVSKIĬ

Moscow State University

Submitted to JETP editor May 19, 1962

J. Exptl. Theoret. Phys. (U.S.S.R.) **43**, 1253-1261 (October, 1962)

Probe and spectroscopic techniques have been used to investigate the deionization of a helium plasma in a uniform longitudinal magnetic field. Calculations of the number of electrons captured at various levels in the He atom show that when $H > 1000$ Oe, $n_e \geq 2 \times 10^{11} \text{ cm}^{-3}$ and $p < 0.1$ mm Hg, the charged particles are lost primarily by volume recombination due to three-body collisions: $\text{He}^+ + 2e \rightarrow \text{He}' + e$. The recombination coefficient and its dependence on electron temperature are determined.

INVESTIGATION of the deionization of a low-density helium plasma^[1] has shown that the magnetic field has a considerably weaker effect on the plasma decay rate than would be expected from ambipolar diffusion due to binary collisions with neutral molecules. At some value of the field the plasma deionization time constant becomes essentially independent of H . Further investigations^[2] indicate that the effect is associated with volume loss processes.

Anomalously rapid loss of plasma in a magnetic field has also been observed by Golant and Zhilinskiĭ^[3] at high charge densities. These authors, however, propose another explanation, namely that diffusion to the walls is enhanced as a consequence of electron-ion collisions.

The present work was undertaken to make direct observations of volume recombination, to establish its role in the deionization of a plasma in a magnetic field, and to evaluate various possible recombination mechanisms.

1. METHOD OF OBSERVATION AND APPARATUS

The decaying plasma was studied in two ways: by probe measurements and by optical measurements. The first method provides the possibility of measuring the change in ion density n_e ¹⁾ while the second gives the possibility of evaluating the corresponding change in the intensity of the recombination radiation I .

A block diagram of the apparatus is shown in Fig. 1. After careful outgassing and evacuation

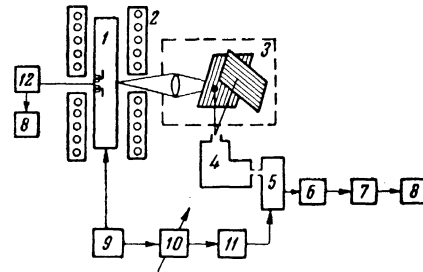


FIG. 1. Block diagram of the apparatus: 1) discharge tube, 2) solenoid, 3) optical system, 4) monochromator, 5) photomultiplier, 6) cathode follower, 7) diode limiter, 8) oscilloscopes, 9) rf generator, 10) delay line, 11) photomultiplier power supply, 12) probe circuit.

to a pressure of 2×10^{-7} mm Hg the discharge tube ($d = 3$ cm, $l = 30$ cm) is filled with spectrally pure helium. The plasma is produced by a pulsed radio-frequency generator (pulse length $15 \mu\text{sec}$, carrier frequency 75 Mc, and pulse repetition rate 50 cps). The tube is located in a solenoid capable of producing uniform magnetic fields up to 2000 Oe. A negative potential (-90 V) is applied to a cylindrical probe ($d = 0.02$ mm, $l = 1.0$ cm) located along the axis of the tube; the probe current is observed with an oscilloscope.

An image of the discharge tube is projected through a gap in the center of the solenoid onto the input slit of a monochromator by means of a mirror system; the image of the tube axis is parallel to the slit of the device. By displacing the image perpendicularly to the slit one can measure the intensity of the plasma emission along the radius of the tube. The radiation is detected with a photomultiplier; the photomultiplier signal is applied to a cathode follower and then to an oscillo-

¹⁾We assume everywhere that the density of positive ions equals the density of electrons: $n_p = n_e$.

scope. Because of the large difference in intensity in the discharge and in the afterglow the power supply is designed so that the full photomultiplier voltage is not applied until after the discharge is terminated. This is accomplished by means of a delay line through which the trigger signal from the rf generator is applied.

By using diode limiters in the probe circuit and in the photomultiplier and by varying the probe resistance and the photomultiplier voltage it is possible to carry out measurements over wide ranges of charge density and intensity. The optical system is calibrated in absolute radiation units and the spectral sensitivity of the photomultiplier is determined by means of a standard incandescent lamp.

The spectroscopic measurements were carried out in the region 3800–7000 Å. The accuracy of the oscilloscope measurements approximately 20%.

2. ANALYSIS OF THE EXPERIMENTAL DATA

Using the measured value of the total probe current i_p we can estimate the density of charged particles in the plasma n_e using the Bohm formula [4]

$$i_p = 0.4n_e S \sqrt{2kT_e / m_+}, \quad (1)$$

where S is the collecting surface, which is determined by the space charge sheath around the probe, while m_+ is the ion mass. The sheath radius is estimated with the Langmuir-Blodgett tables. [5] The measurement of electron temperature T_e in the afterglow, which is of extreme importance in the present work, will be considered in detail below.

Since the optical data must agree with the probe data for the axial region of the plasma, one must calculate the volume density of radiation $I(r)$. The radiation E from a slice of the column is measured directly; this slice is selected by the slit in the monochromator (Fig. 2, cross hatched region); successive positions of the slit overlap. The analysis is not carried out by the Hermann

technique, which is difficult; instead, the following simpler procedure is used. The cylindrical plasma column of height $h = 1$ cm is broken up into n concentric regions; the thickness of each region is equal to the width of the slit. Within each region the charged particles and radiation are assumed to be distributed uniformly. Thus we can write

$$E_m = I_m h \Delta S_{mm} + 2 \sum_{k=m+1}^n I_k h \Delta S_{mk},$$

where ΔS_{mk} is the area of the k -th circular region in the m -th layer. Similarly we can write a system of n equations whose solution will be the volume densities of radiation I_1, I_2, \dots, I_n . As a preliminary step the calculation of areas was carried out for $n = 20$.

3. RESULTS

In Fig. 3 we show the variation of ion density in the afterglow. The enhanced loss of particles for $n_e > 10^{11} \text{ cm}^{-3}$ occurs because of nonlinear effects such as recombination or Coulomb interaction of charged particles. The coincidence of the upper parts of the curve at $H > 1000$ Oe indicates that nonlinear effects, which are independent of magnetic field, predominate over diffusion. This is equivalent to the presence of the plateau on the $\tau(H)$ curve that has been investigated by Golubev. [6]

Spectrophotometric observations of the He I line show that the intensity in the afterglow falls very rapidly to zero when $H = 0$. When the magnetic field is switched on, several hundred microseconds after the termination of ionization a num-

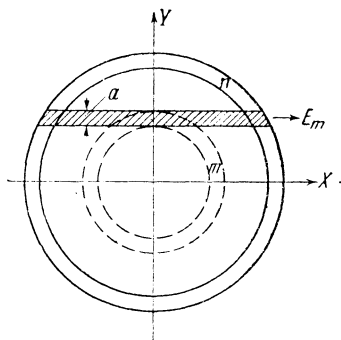


FIG. 2. Diagram used in computing the volume density of radiation: the slit of the apparatus is parallel to the Z axis; X is the direction to the slit.

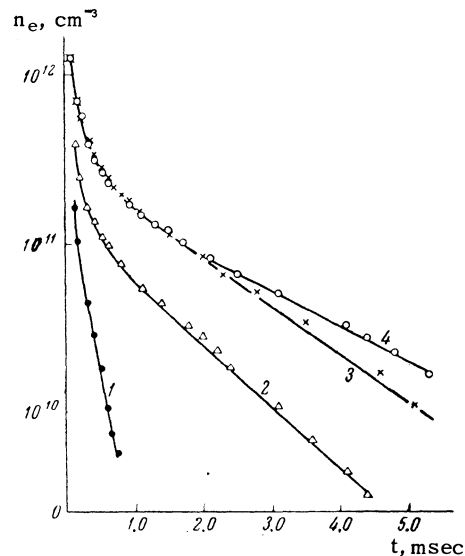


FIG. 3. Variation of ion density in the afterglow: curve 1) $H = 170$ Oe; 2) $H = 510$ Oe; 3) $H = 1190$ Oe; 4) $H = 1530$ Oe (here and below in Figs. 4–8, $p = 6 \times 10^{-2}$ mm Hg).

ber of lines exhibit new maxima; subsequently the intensity falls off slowly over a period of 1–2 mil-
lilsec. When the field is increased to 1000–1500
Oe the intensity of the lines increases many times
and the maxima move closer to the beginning of the
afterglow. When $H > 1500$ Oe there is no further
increase in intensity. The electron temperature
in the after glow is too low (Sec. 4) for the exci-
tation of atoms by electron impact so that the ob-
served radiation can only be the result of electron-
ion recombination with the formation of excited
atoms.

Typical curves of the function $I(r, t)$ are shown
in Figs. 4 and 5. Since each photon is associated
with a single recombination event, a measurement

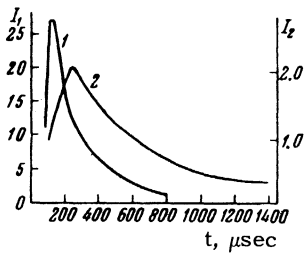


FIG. 4. Variation in intensity of the recombination radiation with time: curve 1) $r = 0$; 2) $r = 12$ mm ($H = 1530$ Oe).

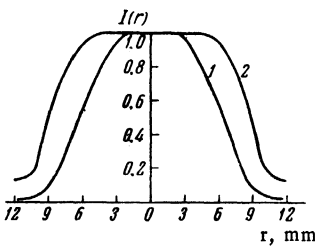


FIG. 5. Distribution of emission intensity over radius: curve 1) $t = 160$ μ sec; 2) $t = 660$ μ sec ($H = 1530$ Oe).

Table I

$\lambda, \text{\AA}$	Transition	$10^{-10} U_\nu / h\nu, \text{cm}^{-3}$
6678	$2^1P - 3^1D$	5.75
5875	$2^3P - 3^3D$	18.9
5015	$2^1S - 3^1P$	1.06
4921	$2^1P - 4^1D$	2.68
4713	$2^3P - 4^3S$	1.5
4471	$2^3P - 4^3D$	8.1
4388	$2^1P - 5^1D$	1.0
4144	$2^1P - 6^1D$	0.21
4121	$2^3P - 5^3S$	0.42
4026	$2^3P - 5^3D$	3.4
3888	$2^3S - 3^3P$	2.34
\sum_λ		45.4

of the absolute energy of the radiation can be used
to compute the number of recombining particles.
Using the $I(r, t)$ curve (Fig. 4) with $r = 0$ we de-
termine the total energy for each line

$$U_\nu = \int_{t_0}^{\infty} I(0, t) dt,$$

radiated in all directions from one cubic centi-
meter in the afterglow starting at $t_0 = 200$ μ sec
as well as the corresponding number of recombina-
tion capture events $U_\nu / h\nu$. In Table I we pre-
sent these data for all the lines that were studied
(very weak lines were not subject to photometric
analysis) with $H = 1530$ Oe and $p = 6 \times 10^{-2}$ mm
Hg. The values of $\sum U_\nu$ and $\sum U_\nu / h\nu = N_r$ (summed
over all lines) and the ratio N_r / n_{e0} , where n_{e0}
is the initial ion density at $t = t_0$, are given in
Table II.

Table II

$p, \text{mm Hg}$	H, Oe	$\sum U_\nu, \text{erg cm}^{-3}$	$10^{-10} N_r, \text{cm}^{-3}$	N_r / n_{e0}	N_r / n_{e0} after [2]
0.06	0	$<10^{-4}$	<0.001	$<10^{-5}$	
	255	$2.4 \cdot 10^{-3}$	0.062	$5 \cdot 10^{-3}$	
	340	$1.7 \cdot 10^{-2}$	0.45	$4 \cdot 10^{-2}$	
	425	$4.6 \cdot 10^{-2}$	1.2	$9.4 \cdot 10^{-2}$	
	510	$7.7 \cdot 10^{-2}$	2.0	0.1	0.8
	680	0.37	9.6	0.19	
	850	0.58	15	0.27	0.87
	1190	1.5	39	0.65	
	1530	1.75	45.4	0.76	0.9
0.1	0	$<10^{-4}$	<0.001	$<10^{-5}$	
	340	$1.6 \cdot 10^{-2}$	0.42	$1 \cdot 10^{-2}$	
	510	0.11	2.8	$6 \cdot 10^{-2}$	
	850	0.58	15	0.16	0.62
	1190	0.88	23	0.2	0.74
	1360	1.3	35	0.35	
	1530	1.4	37	0.37	0.83
	2040	1.6	42	0.42	
0.3	0	$<10^{-4}$	<0.001	$<10^{-5}$	
	340	$6.9 \cdot 10^{-3}$	0.18	$4 \cdot 10^{-3}$	
	425	$2.8 \cdot 10^{-2}$	0.73	$1.4 \cdot 10^{-2}$	
	680	0.2	5.3	$5.9 \cdot 10^{-2}$	0.46
	850	0.46	12	$8.0 \cdot 10^{-2}$	0.58
	1190	0.77	20	0.13	
	1530	1.1	28	0.19	0.58
	2040	1.15	29	0.19	

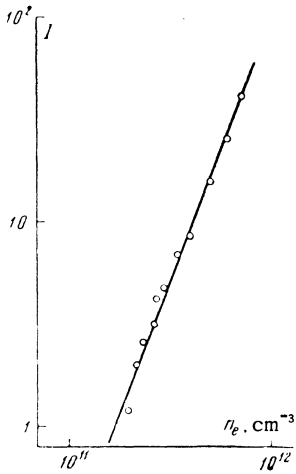


FIG. 6. The intensity of recombination emission as a function of ion density ($H = 1190 - 1530$ Oe).

In Fig. 6, we show on a log-log scale the relation between the radiation intensity and the charge density. The dependence is found to be exponential with an exponent value $\sim 2.6 \pm 0.1$.

4. DECAY OF ELECTRON TEMPERATURE IN THE AFTERGLOW

The change in electron temperature T_e during plasma decay must be known to compute the density n_e using (1) and for the discussion that follows. Using a double floating probe we find $T_e \sim 0.6-0.7$ eV at $t = 40$ μ sec. The accuracy of the measurements is found to be inadequate in colder plasmas and this makes it necessary to carry out the appropriate calculations.

Assuming that the ions are in thermal equilibrium with the neutral gas we take account of the following factors that enter into the variation of T_e : 1) cooling of electrons in elastic collisions with atoms and Coulomb collisions with ions and 2) heating of electrons in superelastic collisions with metastable atoms. From energy conservation we find^[7]

$$\frac{dT_e}{dt} = -\kappa(T_e - T_g)(\nu_{eg} + \nu_{ei}) + \frac{2}{3}n_m\sigma_{em}v_e U_m, \quad (2)$$

where κ is the fraction of energy transferred by an electron in each collision; n_m and U_m are respectively the density and energy of the metastable atoms; σ_{em} is the cross section for a superelastic collision.^[8]

$$\nu_{eg} = 1.24 \cdot 10^7 T_e^{-1/2} p; \quad \nu_{ei} = \frac{5.5 n_e}{T_e^{3/2}} \left\{ \ln \frac{280 T_e}{n_e^{1/2}} + \frac{1}{3} \ln \frac{T_g}{T_e} \right\}.$$

A calculation shows that the metastable states in the discharge vanish in the first few tens of microseconds of the afterglow. However, a rather large value of n_m can persist for a long time by virtue of recombination since approximately $3/4$ of the re-

combining electrons occupy the metastable 2^3S level, which has an energy $U_m = 19.8$ eV (Table I).

The equation for the balance of the number of metastable atoms in this case is

$$\frac{dn_m}{dt} = n_m \left(\frac{1}{\tau_{em}} + \frac{1}{\tau_d} \right) = \frac{3}{4} \frac{dn_e}{dt},$$

where τ_{em} and τ_d are the lifetimes of the metastable states for collisions of the second kind and for diffusion to the walls. It is assumed in this case that the deionization rate dn_e/dt is determined completely by recombination. This assumption holds when $p = 6 \times 10^{-2}$ mm Hg and $H > 1000$ Oe. In other cases one must introduce the corrections using Table II. Furthermore,

$$\frac{1}{\tau_{em}} = n_e \sigma_{em} v_e, \quad \frac{1}{\tau_d} = \frac{D_m}{R^2} = \frac{\lambda_m v_m / 3}{R^2 / 2.4^2} = \frac{1.92 v_m}{R^2 \sigma_{gm} n_g},$$

where $R = 1.5$ cm is the tube radius.

Thus,

$$\frac{3}{4} \frac{dn_e}{dt} = n_m \left(n_e \sigma_{em} v_e + \frac{1.92 v_m}{R^2 \sigma_{gm} n_g} \right), \quad (3)$$

where $\sigma_{gm} = 3.4 \times 10^{-15}$ cm²;^[9] $\sigma_{em} = 8 \times 10^{-17}$ cm²^[10,11].

Equation (2) is integrated numerically using n_m from (3) and the experimentally determined initial value of T_e . However, the required values of n_e can be obtained only from (1) which, in turn, requires a knowledge of T_e . Hence, T_e is determined from (2) and (1) by successive approximations; the zeroth approximation is taken as the values of T_e calculated taking account of only elastic collisions with atoms. The results of this calculation and several experimental points are shown in Fig. 7. The plasma is completely thermalized approximately 250 μ sec after the current stops.

5. DISCUSSION OF THE RESULTS

It follows from Table II that volume recombination is the chief mechanism for removal of charged particles when $p < 0.1$ mm Hg and $H > 1000$ Oe. In this case $n_e > 10^{11}$ cm⁻³. For purposes of compar-

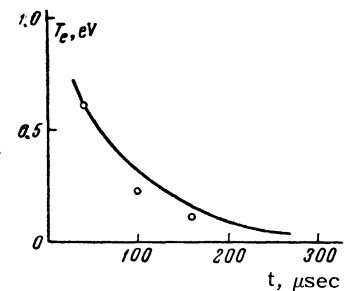


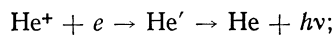
FIG. 7. Variation of electron temperature in the afterglow: the points denote the experimental values while the solid curve denotes the theoretical values ($H = 1530$ Oe).

ison, in the last column of Table II we show the results of Syrgii and Granovskii^[2] obtained under almost analogous conditions by measurement of the integrated ion current to the walls. The agreement is completely satisfactory at large values of H . It should be noted that in the present work we have measured the visible radiation only and for this reason the figures given in the table may be somewhat low.

The rectangular distribution of emission over the diameter (Fig. 5) is also indicative of volume recombination. Since recombination takes place most rapidly at the axis (large value of n_e) the distribution becomes more and more uniform in the course of time.

In order to determine the primary recombination mechanism we consider the following possible processes:

1) Radiative capture



2) Dissociative recombination



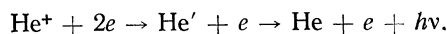
3) Three-body recombination: a) with a neutral particle



b) with a second ion



c) with a second electron



Negative ions cannot be formed in an electro-positive gas such as He and recombination of ions is excluded.

In case 1) the recombination coefficient (summed over all levels) is less than $3 \times 10^{-12} \text{ cm}^3 \text{ sec}^{-1}$ at room temperature.^[12] With $n_e \sim 10^{12} \text{ cm}^{-3}$ the relative deionization rate is $n_e^{-1} dn_e/dt = \alpha n_e \approx 3 \text{ sec}^{-1}$, which is 3–4 orders of magnitude smaller than the observed value (cf. Fig. 3).

The recombination process described in 2) has been considered in a rather large number of experimental and theoretical papers;^[13,14] these yield a value of α sufficiently large to explain the observed recombination rate. However there are a number of serious objections against this process under our conditions. Mass spectrometer investigations^[15] show that the density of molecular ions is less than 10% in a stationary discharge at pressures below 1 mm Hg. A simple calculation for the formation of molecular ions in the afterglow

(using the appropriate experimentally determined coefficients^[16]) shows that during the first several milliseconds the density of molecular ions is appreciably smaller than the density of atomic ions. Furthermore, dissociative recombination cannot explain the observed population of the higher levels of He with $U_i \approx 0.5 \text{ eV}$. On the other hand, for the highest excited states resulting from recombination one expects that U_i will exceed 2.2 eV, the dissociation energy of the molecular ion.^[17] In order to avoid this contradiction it may be assumed that the molecular ions are in metastable states;^[18] however, experiments we have carried out adding approximately 0.1% of Ar as an impurity to He (for quenching the metastable states) give results the same as those described above.

The process described in 3a) is not very probable at low pressures; the cross section for this process is proportional to pressure and this does not agree with present measurements (Table II).

Considering processes 3b) and 3c) we find the latter is much more effective^[19] and for this reason it is considered here. D'Angelo^[20] has calculated the recombination coefficient for 3c) taking account of electron capture in excited levels; the values of α that are obtained exceed the coefficient for radiative capture by 1–2 orders of magnitude. In this case the recombination rate is

$$dn_e/dt = -\alpha n_e^k, \quad (4)$$

where k varies from 2.65 to 2.4 as T_e changes. Taking account of cascade processes gives a still higher value of α for He;^[21] Extrapolation to conditions of the present work gives a recombination time constant $\tau \approx 250 \mu\text{sec}$ for $n_e = 5 \times 10^{11} \text{ cm}^{-3}$, in good agreement with our results (Fig. 3). Calculation and experiments carried out on the stellarator^[10] give $k = 2.5$.

Since the intensity of the recombination radiation is $I = h\nu dn_e/dt$, taking account of (4) we have

$$I = h\nu \alpha n_e^k, \quad \log I = \text{const} + k \log n_e. \quad (5)$$

Thus, k coincides with the slope of the line Fig. 6: $k = 2.6 \pm 0.1$. Integrating (4) and substituting the value of k that has been obtained we find

$$n_e^{-1.6} - n_{e0}^{-1.6} = 1.6\alpha (t - t_0).$$

The dependence of the quantity $n_e^{-1.6}$ on time is shown in Fig. 8. The linear behavior of the curve up to $t = 1.5 \text{ msec}$. indicates that the recombination mechanism for the removal of charges is maintained in this range. The recombination coefficient found in this way is $\alpha = 8.6 \times 10^{-16}$, corresponding to $T_e = 0.03 \text{ eV}$.

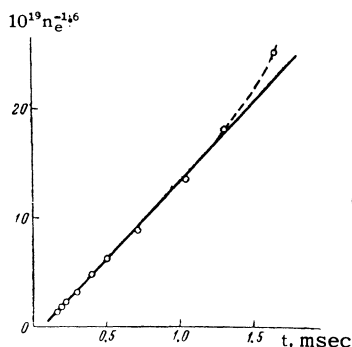


FIG. 8. The electron density as a function of time ($H = 1530$ Oe).

The sharp increase in radiation intensity after the termination of current flow is related to the strong dependence of the recombination coefficient on electron temperature. The same effect is responsible for the appreciable shift in time of the maximum radiation from the axial and peripheral zones of the column (Fig. 4). Knowing the variation of T_e in time (Fig. 7) we can find the function $\alpha(T_e)$ from the following considerations. From Eq. (5) we obtain the condition for maximum intensity:

$$-\left(\frac{d\alpha}{dt}\right)_m n_{em}^k = k\alpha_m n_{em}^{k-1} \left(\frac{dn_e}{dt}\right)_m,$$

where the subscript m denotes values of the appropriate quantities for $t = t_{\max}$. We write α in the form $\alpha = c/T_e^\beta$, thus obtaining

$$\beta \left(\frac{1}{T_e} \frac{dT_e}{dt}\right)_m = k \left(\frac{1}{n_e} \frac{dn_e}{dt}\right)_m, \quad \beta = k \frac{\vartheta_m}{\tau_m},$$

where ϑ_m and τ_m are the time constants for the variation in T_e and n_e . From Figs. 3 and 7 we find $\beta = 2.8 \pm 0.2$. In the work of D'Angelo^[20] this quantity was estimated as $\beta = 2.5$, while Kuckes and Motley^[10] estimate $\beta = 3$.

Below we give values of the recombination time constant τ_r for various densities n_e calculated from (4) using the values found for α and k and the deionization time constant of the plasma τ determined from Fig. 3 with $H > 1000$ Oe:

$10^{-11}n_e, \text{ cm}^{-3}$:	8	6	4	3	2	1	0.7
$\tau_r, \mu\text{sec}$:	105	165	320	500	970	2900	5200
$\tau, \mu\text{sec}$:	130	220	370	540	1000	1600	2050

When $n_e > 2 \times 10^{11} \text{ cm}^{-3}$ the removal of charged particles is explained completely by volume recombination. At lower values of n_e recombination cannot provide the observed deionization rate and the principal mechanism is diffusion to the walls. In this connection we can understand the origin of the discrepancy of the results in ^[2] and ^[3]: in the latter case $n_e < 10^{11}$ and volume recombination could not be observed.

CONCLUSIONS

1. A decaying helium plasma in a uniform magnetic field emits intense afterglow radiation consisting of spectral lines of He I; these lines are excited by electron recombination in higher states.

2. A calculation of the number of free electrons captured in excited levels of He and causing radiation in the visible region, shows that volume recombination increases with increasing magnetic field and with reduced pressure; when $H > 1000$ Oe, $p < 0.1$ mm Hg and $n_e \geq 2 \times 10^{11} \text{ cm}^{-3}$ the chief mechanism for the removal of charged particles is volume recombination.

3. When $n_e < 10^{11} \text{ cm}^{-3}$ and $H < 2000$ Oe volume recombination has an insignificant effect on the deionization rate of the plasma.

4. Recombination proceeds primarily by a three-body collisions (electron, electron-ion); the deionization due to this effect is given by the relation

$$dn_e/dt = -4.7 \cdot 10^{-20} n_e^k / T_e^\beta,$$

where $k = 2.6 \pm 0.1$, $\beta = 2.8 \pm 0.2$.

¹A. S. Syrgiĭ and V. L. Granovskii, Radiotekhnika i elektronika (Radio Engineering and Electronics) **4**, 1854 (1959).

²A. S. Syrgiĭ and V. L. Granovskii, Radiotekhnika i elektronika **5**, 1522 (1960).

³V. E. Golant and A. P. Zhilinskiĭ, ZhTF **30**, 745 (1960). Soviet Phys. Tech. Phys. **4**, 670 (1960).

⁴A. Guthrie and P. K. Wakerling, The Characteristics of Electrical Discharges in Magnetic Fields, N. Y., McGraw-Hill, 1949, p. 14.

⁵I. Langmuir and K. B. Blodgett, Phys. Rev. **22**, 347 (1923).

⁶V. S. Golubev, Radiotekhnika i elektronika **7**, 153 (1962).

⁷V. L. Granovskii, ZhTF **13**, 123 (1943).

⁸V. L. Ginzburg, Rasprostranenie elektromagnitnykh voln i plazme (Propagation of Electromagnetic Waves in Plasma), M., Gostekhizdat, p. 62.

⁹A. V. Phelps and J. P. Molnar, Phys. Rev. **89**, 1204 (1953).

¹⁰A. F. Kuckes and R. W. Motley, Fifth International Conference on Ionization Phenomena in Gases, Munich, 1961.

¹¹G. J. Schulz and R. E. Fox, Phys. Rev. **106**, 1179 (1957).

¹²H. S. L. Massey and E. H. S. Burhop, Electron and Ion Impact Phenomena, (Russ. transl.) IIL, 1958, p. 287. (Oxford Univ. Press, 1952).

¹³D. R. Bates, Phys. Rev. **77**, 718 (1950); **78**, 492 (1950).

¹⁴M. A. Biondi and S. C. Brown, Phys. Rev. **76**, 1697 (1949).

¹⁵D. Morris, Proc. Phys. Soc. **A68**, 11 (1955).

¹⁶Johnson, McClure, and Holt, Phys. Rev. **80**, 376 (1950).

¹⁷M. A. Biondi and T. Holstein, Phys. Rev. **82**, 962 (1951).

¹⁸M. A. Biondi, Phys. Rev. **83**, 1078 (1951).

¹⁹V. L. Granovskiĭ, Elektricheskiĭ tok v gaze

(Electrical Currents in Gases) Vol. 1, Fizmatgiz, 1962, p. 176.

²⁰N. D'Angelo, Phys. Rev. **121**, 505 (1961).

²¹E. Hinnov and J. G. Hirschberg, Fifth International Conference on Ionization Phenomena in Gases, Munich, 1961.

Translated by H. Lashinsky

219